Magnetic field induced spin-wave energy focusing

Noel Perez* and Luis Lopez-Diaz
Department of Applied Physics, University of Salamanca, Plaza de los Caidos s/n 37008, Salamanca, Spain
(Received 19 December 2014; revised manuscript received 15 June 2015; published 9 July 2015)

Local temperature variations induced by spin-wave propagation are studied using a model that couples nonuniform magnetization dynamics and heat flow. We show that the remote heating at the sample edge reported recently [T. An *et al.*, Nat. Mater. **12**, 549 (2013)] is due to the geometry-induced gradual reduction of the effective field. We demonstrate that the same effect can be achieved by a reduction in the external field instead of a constriction at the edge and, furthermore, that both the location and the amount of energy to be delivered to the lattice can be controlled accurately this way.

DOI: 10.1103/PhysRevB.92.014408 PACS number(s): 75.30.Ds, 75.40.Gb, 75.40.Mg, 75.78.Cd

I. INTRODUCTION

The capacity of spin waves to transport both energy and angular momentum as they propagate in a magnetic medium is at the heart of the emerging fields of spin caloritronics [1] and magnon spintronics [2]. To successfully translate the fundamental research in these fields to technology, it is crucial to be able to manipulate the flow and delivery of energy carried by spin waves in a controllable and flexible way over different length scales. Since spin-wave propagation is mostly governed by intrinsic relaxation mechanisms in the material, strong efforts are being made to develop samples with very low intrinsic damping coefficient [3] or to partially compensate damping by means of current-induced torques [4,5] or thermal gradients [6]. These approaches might lead to a global increase in the propagation length of spin waves, but their amplitude decays exponentially as moving away from the source. For energy-efficient applications, however, it would be desirable to be able to convey large amplitude spin-wave oscillations to specific regions. In a recent paper, An and coworkers [7] took a first step in this direction. In particular, they showed that the nonreciprocal nature of magnetostatic surface spin waves (MSSW) [8,9] allows for controllable unidirectional spin-wave propagation and, moreover, for remote heating at the sample edge towards which the spin waves propagate. The mechanism by which the spins pump energy to the lattice leading to remote heating of the sample is, however, not well understood yet [7].

In the present work, we use micromagnetic simulations to demonstrate that a large amount of the energy carried by surface spin waves can be efficiently conveyed to a small area by gradually reducing the effective field at the target region. The mechanism is rather simple. As the field decreases so does the group velocity of the spin waves, and the wave packet starts compressing. At some point, the field reaches a value for which they cannot propagate further, and we observe an increase in the amplitude of the oscillations, which results into localized heating and spin accumulation. We show that the experimental results in Ref. [7] can be quantitatively explained within our general scheme considering the decrease in the effective field due to the gradual width reduction at the sample edge. Consequently, we unveil the mechanism by which the spins pump energy to the lattice in Ref. [7] and, in passing, we propose a general and flexible scheme for focusing the energy flow in a ferromagnet.

II. MODEL AND SPECIFICATIONS

In this paper, we study theoretically the local variations of the lattice temperature induced by nonuniform magnetization dynamics in the sample. To do that, we have developed a model that couples magnetization dynamics and heat flow in a thermodynamically consistent way, allowing us to simulate real-time temperature fluctuations. Our model is meant for magnetic insulators and it assumes that electrons and phonons are in local equilibrium at every moment in time. Consequently, they are considered as a single system referred to as "the lattice." The magnetization dynamics is given by the standard Landau-Lifshitz-Gilbert equation

$$\frac{d\boldsymbol{m}}{dt} = -\gamma\, \boldsymbol{m} \times (\boldsymbol{B}_{\text{eff}} + \boldsymbol{B}_{\text{th}}) + \alpha\, \boldsymbol{m} \times \frac{d\boldsymbol{m}}{dt}, \qquad (1)$$

where $\boldsymbol{m}(\boldsymbol{r},t)$ is the reduced magnetization, γ is the gyromagnetic ratio, α is the damping parameter, $\boldsymbol{B}_{\text{eff}}$ is the effective field (including exchange, anisotropy, self-magnetostatic and Zeeman contributions), and $\boldsymbol{B}_{\text{th}}$ is the random field representing thermal fluctuations [10]. On the other hand, the thermal properties of the lattice are macroscopically described by its temperature distribution, which changes in space and time according to the heat equation

$$\frac{dT}{dt} = \frac{1}{c_p \rho}\left(\kappa\, \nabla^2 T + M_s \frac{d\boldsymbol{m}}{dt} \cdot \boldsymbol{B}_{\text{eff}} + q_{\text{ext}}\right), \qquad (2)$$

where T is the temperature, κ the thermal conductivity, c_p the specific heat capacity, ρ the density, M_s the saturation magnetization, and $\boldsymbol{B}_{\text{eff}}$ the total effective field acting on the system. The first term accounts for phonon-phonon interactions as a diffusive term, which tends to make the temperature uniform, in a similar way as the exchange does for the spin system. The second term represents heat transfer between the spins and the lattice, computed as the variation of magnetic energy of the spin system. The last term describes heat transfer per unit volume and time between the lattice and the environment. In the present work, we consider a standard Newton term $q_{\text{ext}} = c_p \rho \frac{T_0 - T}{\tau}$, T_0 being the room temperature and τ the characteristic thermal relaxation time constant. Equations (1) and (2) are solved self-consistently, the

*noelpg@usal.es

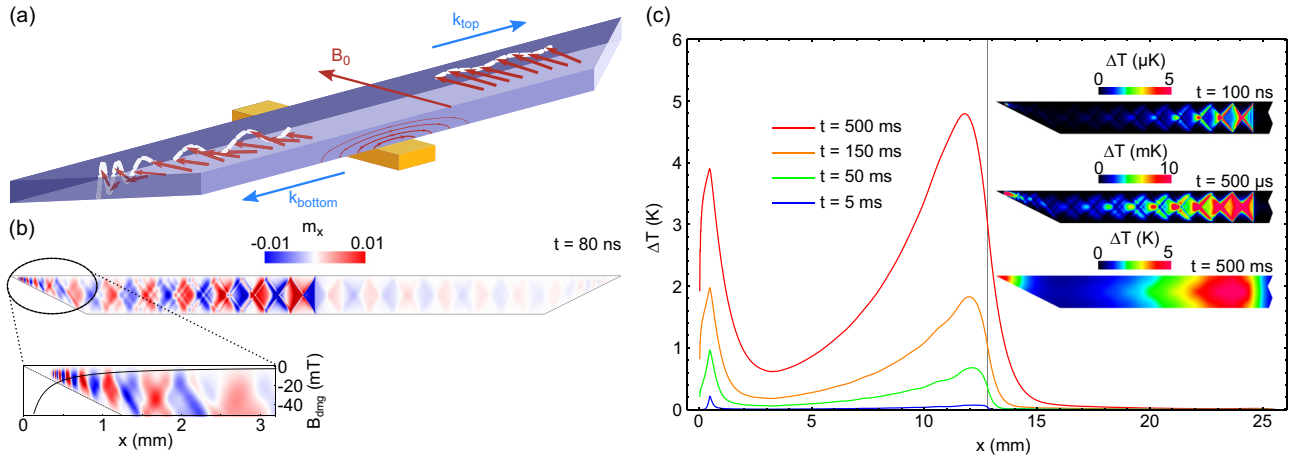

FIG. 1. (Color online) Geometric control of spin-wave energy dissipation. (a) Schematic representation of the studied system. (b) Magnetic configuration in the inner layer of the sample (12 μm from the bottom) after a time of 80 ns for a continuous microwave excitation at a frequency of 7 GHz. The profile of the internal demagnetizing field in the y direction is shown below, overlaid on a close-up of the magnetic configuration. (c) Time evolution of the temperature profile of the system. (Inset) Temperature maps of the propagation region at different times.

temperature distribution entering (1) in the amplitude of the thermal field [10].

The system under study is intended to closely mimic one of the experiments in Ref. [7]. We consider a 25.6 mm $\times$ 1.6 mm $\times$ 32 μm sample with its edges cut at a sharp angle of 30° and magnetized in the y direction by a uniform external field $B_0 = 175$ mT [see Fig. 1(a)]. We used the following single-crystalline YIG magnetic parameters: gyromagnetic ratio $\gamma = 1.76 \times 10^{11}$ rad T^{-1} s^{-1} [7], saturation magnetization $M_s = 1.45 \times 10^5$ A m^{-1} [7], exchange constant $A = 1.0 \times 10^{-11}$ J m^{-1}, and damping constant $\alpha = 5.0 \times 10^{-4}$. Note that even though the exchange constant is higher than the typically measured one ($A = 3.7 \times 10^{-12}$ J m^{-1} [11]), exchange plays a very small role in our sample due to its large size, and does not affect the outcome of our simulations for a wide range of values of the exchange coupling constant. On the other hand, the thermal behavior was obtained using $\alpha_{\text{th}} = \frac{\kappa}{\rho c_p} = 1.5 \times 10^{-6}$ m^2 s^{-1}, $\kappa = 8$ W m^{-1} K^{-1}, $\tau = 1.0$ s, and $T_0 = 300$ K for the thermal diffusivity, thermal conductivity, characteristic time constant, and room temperature, respectively (see Ref. [12] and references therein for various measures of α_{th} and κ). The sample was discretized in 12.5 μm $\times$ 12.5 μm $\times$ 8.0 μm cells. The use of such large cells as compared to the exchange length ($\sqrt{\frac{2A}{\mu_0 M_s}} = 27.5$ nm) is justified because the characteristic wavelength of excited MSSW is of the order of hundreds of micrometers, and short-range exchange effects can be neglected over such long distances.

III. RESULTS AND DISCUSSION

MSSW are excited in the central region with an ac current of amplitude $I_0 = 18.7$ mA and frequency $f = 7.0$ GHz along a 50-μm wide antenna placed underneath the film [see Fig. 1(a)]. Figure 1(b) shows the magnetic configuration of the system after $t = 80$ ns. As can be observed, propagation is mostly unidirectional due to (i) nonreciprocal displacement of MSSW [9,13] and decay of the ac field amplitude as moving away from the antenna cause the waves in the bottom surface, moving to the left, to be excited with a higher amplitude ac field than the ones in the top surface, which move to the right, and (ii) interference between spin waves excited at the right and left sides of the antenna, which have opposite out-of-plane components of the ac magnetic field, is constructive on the left direction of propagation and destructive on the right one [14]. The magnetization pattern observed, particularly in the area closer to the antenna, is characterized by periodic standing maxima and minima of the spin-wave amplitude, and it is attributed to the interference between spin-wave modes with different quantized transversal wave vectors [15,16]. Furthermore, the amplitude of the MSSW decays exponentially as moving away from the source due to magnetic damping. At the edge, however, we observe that both the wavelength and group velocity are gradually reduced (see zoomed in region in Fig. 1(b) and movie 1 in Ref. [17]), while the amplitude increases. It is worth noting that this energy accumulation occurs before the spin waves reach the leftmost point of the edge, which indicates that pure geometric confinement is not the underlying cause of this accumulation.

After $t \approx 200$ ns, the amplitude of the oscillations reaches a stationary distribution and, consequently, so does the heat density distribution delivered to the lattice. Therefore, from then on, we evaluate the time evolution of the temperature in the system taking this distribution as an external fixed heat source, which allows us to investigate the thermal behavior of the sample on a time scale in the order of a second, similar to that of the experiments ([7,18]). During the first few milliseconds, the temperature distribution very closely reproduces the pattern of the MSSW amplitude distribution [Fig. 1(c)], but it is smoothed out after a short time due to diffusion, and two temperature peaks become clearly distinguishable, one in the excitation region and the other one at the edge due to the spin-wave accumulation described above. This result is in very good qualitative and reasonable quantitative agreement with Fig. 4 in Ref. [7].

In their paper, An and coworkers propose two possible mechanisms by which the spin waves release their energy to the lattice, spin-wave multireflections at the edge due to the sharp 30° angle cut and two-magnon scattering processes. Multireflections were not observed in our simulations, but rather spin-wave propagation was smooth at the edge, as seen, e.g., in movie 1 in Ref. [17]. Even if the stripe edge is rough, spin-wave scattering due to diffuse reflections plays a small role on spin-wave absorption (see Fig. 1 in Ref. [17]). On the other hand, our simulations do not consider the contribution from two-magnon scattering due to defects and impurities, which may be relevant. The observed phenomena can also be explained from a classical point of view: the reduced width at the edges is responsible for an increase in the demagnetizing field, which consequently reduces the local effective field. This nonuniform effective field is directly related to the propagation characteristics of the spin waves, and a reduction in its magnitude causes a decrease in the spin waves' wavelength and group velocity, leading to the compression of the wave packet. Eventually, the external field is too low for spin waves to be able to propagate further, and the waves, traveling at almost zero speed, accumulate and dissipate their energy in the form of heat.

Therefore the principle underneath the spin-wave energy dissipation is more general than just geometric confinement; it lies on the propagation characteristics of the waves themselves. MSSW can only propagate in a narrow band of frequencies, and this band can be tuned by controlling the magnetic field acting on the system. If the magnetic field is not uniform and varies in space, so will the properties of the spin waves as they propagate. Although propagation of spin waves in nonuniform fields has already been investigated (see, e.g., Refs. [19–23]), most studies have focused on wave vector dispersion, phase shifts or mode localization across the stripe width, whereas spin-wave localized absorption has been given little attention.

To further investigate this effect, we perform our next experiment on a system similar to the one described above, but instead of controlling energy dissipation by cutting the edges at 30° we introduce a spatial variation of the external magnetic field. Namely, we consider a smooth field profile given by $B(x) = B_0 - B_1/\{1 + \exp[\frac{4(x-x_0)}{w}]\}$, where $x_0 = 5.625$ mm, $w = 0.5$ mm, and $B_1 = 17.5$ mT are the center, width, and magnitude of the field variation, respectively [see Fig. 2(a)]. A similar field profile could be experimentally achieved by placing a ferromagnetic stripe at the desired region (see Fig. 2 in Ref. [17]). A 5-ns-long microwave pulse of 7-GHz frequency is applied through the antenna and the time evolution of the excited spin-wave packet is studied.

As in the previous case, the nonreciprocal behavior of MSSW leads to a net transport of energy towards the left. In the excitation region, where $B(x) \approx B_0$, the excitation frequency lies within the range of propagation of MSSW [see inset in Fig. 2(a)]. When the wave packet reaches the region where the magnetic field changes, the surface waves passband is shifted towards lower frequencies [see Fig. 2(a)], and eventually the excitation frequency is left outside the propagation band. As approaching this point, the wavelength and group velocity gradually decrease, leading to localized spin accumulation [Fig. 2(c)] and heating [Fig. 2(d)] as in the previous scenario. Reflections are further hindered for the particular case of MSSW, since the reflected wave has to propagate on the top surface, and low wavelength modes have a pronounced amplitude decay from the bottom surface [9]. In order to quantify this reflection hindering, we performed the same experiment on magnetostatic backwards volume waves (MBVW), which do not have this constraint on reflection (see Fig. 4 in Ref. [17]). For similar excitation and field profile, the obtained reflection coefficients were $R \approx 13\%$ and $\approx 25\%$ for MSSW and MBVW, respectively.

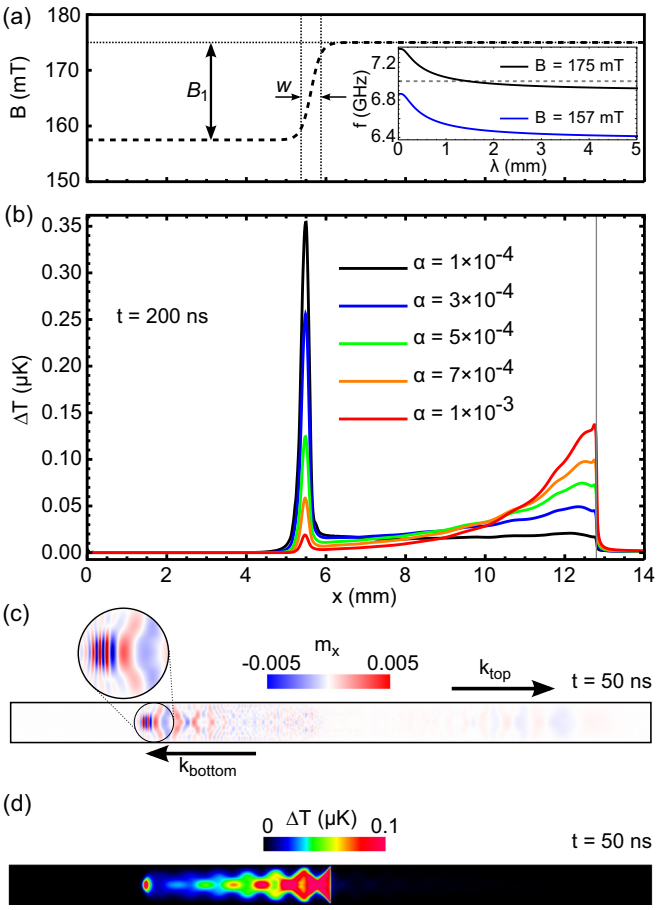

FIG. 2. (Color online) Spin-wave pulse energy focusing by a change in the magnetic field. (a) External field spatial distribution. Inset represents the MSSW dispersion relation in the propagation ($B = 175$ mT) and nonpropagation ($B = 157$ mT) regions. Dashed line in inset represents the excitation frequency (7 GHz). (b) Spatial distribution profile of the increase of temperature as a function of magnetic damping after a time of 200 ns. (c) Magnetic configuration after a time of 50 ns. Bottom surface spin waves propagate leftwards whereas top surface spin waves propagate rightwards. (d) System temperature distribution after a time of 50 ns.

The longitudinal temperature profile at $t = 200$ ns is plotted for different values of the damping constant α in Fig. 2(b), all of them within a realistic range for single-crystalline YIG. We observe a high-temperature spot localized in the region where the field changes, which becomes more pronounced as α decreases. Therefore a suitable smooth variation in the external field reveals itself as an efficient way of conveying spin-wave energy to a particular region.

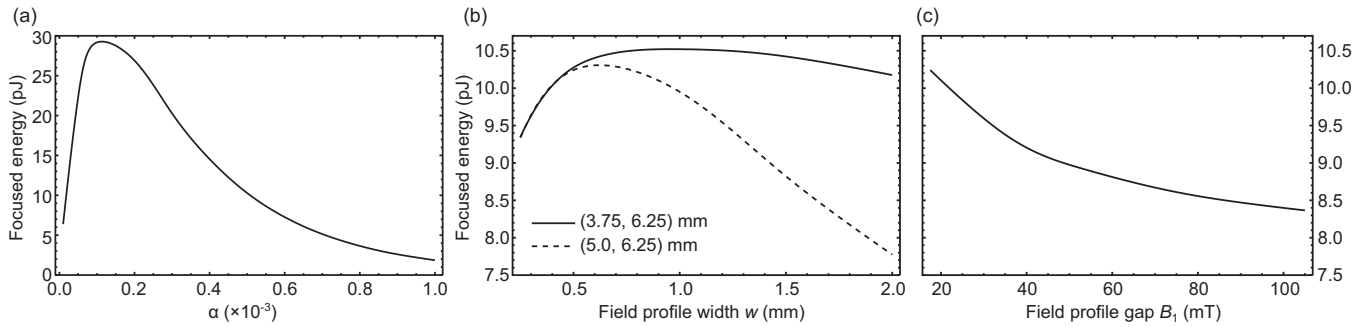

FIG. 3. Energy focusing efficiency with a 5-ns microwave pulse excitation. (a) Energy absorbed at the edge after 200 ns as a function of magnetic damping. (b) Energy absorption efficiency as a function of the width of the magnetic field change region (w). Solid and dashed lines correspond to energy absorbed in the regions 3.75 mm $< x <$ 6.25 mm, and 5.0 mm $< x <$ 6.25 mm, respectively. (c) Energy absorption efficiency as a function of magnetic field change magnitude. In all graphs, the default parameters are $\alpha = 5 \times 10^{-4}$, $w = 0.5$ mm, $B_1 = 17.5$ mm, and total pulse energy is 75 pJ.

IV. EFFICIENCY

To further explore this phenomenon, we analyze its efficiency as a function of both the damping coefficient α and the magnetic field profile parameters w and B_1. As in the previous case, a 5-ns-long microwave pulse is applied. The magnetic energy pumped into the magnetic system by the pulse, computed as the energy absorbed in the whole sample over a sufficiently long time, is $E_{\text{pulse}} \approx 75$ pJ. This value was found to be independent of α. The focusing efficiency, therefore, is given by the amount of energy dissipated in the region where the field changes. The results are presented in Fig. 3. Figure 3(a) shows the energy absorbed in the region 5.0 mm $< x <$ 6.25 mm after 200 ns as a function of α. A well defined maximum at $\alpha \approx 10^{-4}$ is found. Intuitively, a monotonic increase in the efficiency as α decreases would be expected, since lower damping implies less attenuation of the spin waves as moving away from the source. Indeed, this is what we observe for $\alpha > 10^{-4}$. However, a very low damping parameter is also detrimental to the efficiency because a significant amount of energy is reflected back via MSSW in the top surface.

In Fig. 3(b), we show the absorption in both a narrow region (5.0 mm $< x <$ 6.25 mm) and a wider region (3.75 mm $< x <$ 6.25 mm) as a function of the width of the transition region w. The maximum energy dissipated in the narrow region is obtained for $w \approx 0.6$ mm. Below this value both curves coincide, meaning that energy absorption is confined to a small region. For larger values of w, however, where the field variation is more gradual, the two curves diverge, meaning that a significant part of the energy is being absorbed outside the narrow region, resulting in a loss of focus. On the other hand, the efficiency loss for very low values of w observed in Fig. 3(b) is attributed to the fact that, for very abrupt transitions, the reflection coefficient increases. The same decrease in efficiency due to reflections is observed if we increase the field variation magnitude B_1 instead of decreasing the width, as shown in Fig. 3(c). Consequently, some control of the field variation profile is required in order to maximize the energy delivered to the target region. Nevertheless, the method is robust and has a broad range of operation, since deviations from ideal conditions up to 100% result in only a 10% decrease in the efficiency (Fig. 3).

The approach for focusing the spin-wave intensity with a spatially varying magnetic field proposed in this paper is highly efficient because, as seen in Fig. 3(a), up to 40% of the energy pumped into the system can be conveyed to the target region far away from the source. It is also flexible, since it allows for an easy control of both the target region and the amount of energy to be delivered there. Moreover, we have repeated the experiment discussed in Fig. 2 on a system scaled down by a factor of 100 and the same behavior was obtained (see Fig. 3 in Ref. [17]), which indicates that the approach is scalable to a large extent. On the other hand, it is also not limited to MSSW, but it can also be applicable to magnetostatic backward volume waves (MBVW, see Fig. 4 in Ref. [17]), although with a significantly reduced efficiency.

V. CONCLUSION

In summary, we have revealed that the mechanism leading to remote heating of a magnetic stripe via surface spin waves lies on the modification of their dispersion relation by a gradual variation of the geometry or external magnetic field. Based on this, we have proposed a versatile, error-tolerant, and down-scalable method for controlling spin and energy accumulation in magnetic systems. Spin accumulation could generate a transversal spin current in an adjacent layer, or it can dissipate into heat, generating a localized temperature gradient. A maximum efficiency of 40% can be achieved with a simple experimental setup. Understanding and controlling spin-wave flow and delivery is of great importance in spin caloritronics and magnon spintronics and opens the door to new devices such as magnetic transistors or frequency filters.

ACKNOWLEDGMENTS

This work was supported by the regional government (Project SA163A12 from Junta de Castilla y Leon), Spanish government (Project MAT2011-28532-C03-01), and the European Social Fund.

[1] G. E. W. Bauer, E. Saitoh, and B. J. van Wees, Nat. Mater. **11**, 391 (2012).
[2] Y. Kajiwara, K. Harii, S. Takahashi, J. Ohe, K. Uchida, M. Mizuguchi, H. Umezawa, H. Kawai, K. Ando, K. Takanashi, S. Maekawa, and E. Saitoh, Nature (London) **464**, 262 (2010).
[3] O. d'Allivy Kelly, A. Anane, R. Bernard, J. Ben Youssef, C. Hahn, A. H. Molpeceres, C. Carrtro, E. Jacquet, C. Deranlot, P. Bortolotti, R. Lebourgeois, J.-C. Mage, G. de Loubens, O. Klein, V. Cros, and A. Fert, Appl. Phys. Lett. **103**, 082408 (2013).
[4] S.-M. Seo, K.-J. Lee, H. Yang, and T. Ono, Phys. Rev. Lett. **102**, 147202 (2009).
[5] K. Ando, S. Takahashi, K. Harii, K. Sasage, J. Ieda, S. Maekawa, and E. Saitoh, Phys. Rev. Lett. **101**, 036601 (2008).
[6] E. Padron-Hernandez, A. Azevedo, and S. M. Rezende, Phys. Rev. Lett. **107**, 197203 (2011).
[7] T. An, V. I. Vasyuchka, K. Uchida, A. V. Chumak, K. Yamaguchi, K. Harii, J. Ohe, M. B. Jungfleisch, Y. Kajiwara, H. Adachi, B. Hillebrands, S. Maekawa, and E. Saitoh, Nat. Mater. **12**, 549 (2013).
[8] R. W. Damon and J. Eshbach, J. Phys. Chem. Solids **19**, 308 (1961).
[9] D. D. Stancil and A. Prabhakar, *Spin Waves: Theory and Applications* (Springer, Berlin, 2009).
[10] J. L. Garcia-Palacios and F. J. Lazaro, Phys. Rev. B **58**, 14937 (1998).
[11] S. Klinger, A. V. Chumak, T. Mewes, B. Khodadadi, C. Mewes, C. Dubs, O. Surzhenko, B. Hillebrands, and A. Conca, J. Phys. D: Appl. Phys. **48**, 015001 (2015).
[12] K. I. Uchida, T. Kikkawa, A. Miura, J. Shiomi, and E. Saitoh, Phys. Rev. X **4**, 041023 (2014).
[13] K. L. Wong, L. Bi, M. Bao, Q. Wen, J. P. Chatelon, Y.-T. Lin, C. A. Ross, H. Zhang, and K. L. Wang, Appl. Phys. Lett. **105**, 232403 (2014).
[14] A. A. Serga, A. V. Chumak, and B. Hillebrands, J. Phys. D: Appl. Phys. **43**, 264002 (2010).
[15] V. E. Demidov, S. O. Demokritov, K. Rott, P. Krzysteczko, and G. Reiss, Appl. Phys. Lett. **91**, 252504 (2007).
[16] V. E. Demidov, S. O. Demokritov, K. Rott, P. Krzysteczko, and G. Reiss, Phys. Rev. B **77**, 064406 (2008).
[17] See Supplemental Material at http://link.aps.org/supplemental/10.1103/PhysRevB.92.014408 for additional information regarding roughness effects and applicability to real systems.
[18] T. An, K. Yamaguchi, K. Uchida, and E. Saitoh, Appl. Phys. Lett. **103**, 052410 (2013).
[19] W. Faber, Electron. Lett. **16**, 452 (1980).
[20] S. J. Wallin and D. D. Stancil, J. Appl. Phys. **57**, 3718 (1985).
[21] K. R. Smith, M. J. Kabatek, P. Krivosik, and M. Wu, J. Appl. Phys. **104**, 043911 (2008).
[22] S. V. Vasiliev, V. V. Kruglyak, M. L. Sokolovskii, and A. N. Kuchko, J. Appl. Phys. **101**, 113919 (2007).
[23] J. P. Park, P. Eames, D. M. Engebretson, J. Berezovsky, and P. A. Crowell, Phys. Rev. Lett. **89**, 277201 (2002).